Journal of Anatomy

J. Anat. (2017) **230**, pp497–509 doi: 10.1111/joa.12582

A biomechanical view on stinger diversity in scorpions

Arie van der Meijden[1] and Thomas Kleinteich[2]

[1]*CIBIO Research Centre in Biodiversity and Genetic Resources, InBIO, Universidade do Porto, Vila do Conde, Portugal*
[2]*Department of Zoology, Functional Morphology and Biomechanics, Kiel, Germany*

Abstract

Scorpions have elongated metasomas that bear a telson, which is used as a stinger for venom injection. There is a remarkable diversity in the use of the stinger among scorpions, comprising defensive behavior, prey subjugation and mating. This diversity could be reflected by the shape of the telson, as different stinging behaviors will result in very different functional demands. Here we explored the diversity of telson shapes in scorpions by providing morphological measurements, such as curvature and tip angle, as well as by testing stingers under load using finite element analysis (FEA). FEA models were loaded with forces scaled to the surface area of the models, to allow comparison of the relative strain energy based on shape alone. Load force angle was rotated to identify the optimal stinging angle based on the lowest strain energy. Aculeus length and mean aculeus height correlated with minimal strain energy. Optimal stinging angle correlated with tip angle, and differed from the tip angle by about $28.4 \pm 6.22\,^{\circ}$. We found that species that are more venomous have long aculei (stinger barbs) with a larger radius of curvature. FEA models of these longer aculei showed basal stress concentrations, indicating a potential greater risk of basal breakage due to shape alone. Telsons with shorter and thicker aculeus shapes showed stress concentrations at the tip only. Despite these marked differences in shape, we found no difference in the scaled strain energy between groups of species that are more venomous and less venomous groups of species. These results show that scorpion stingers may be biomechanically optimized, and this may indicate different usage of the stinger in different species.

Key words: finite element analysis; injection; scorpions; stingers; venom; μCT.

Introduction

Scorpions use venom to defend themselves from predators, to immobilize prey, in intraspecific antagonism as well as during mating. Venom is injected by the telson, which consists of the sharp aculeus, the bulbous vesicle containing the venom glands and associated musculature, and the peduncle with which it attaches to the last segment of the metasoma (often referred to as 'tail', but actually a continuation of the body). The muscles that move the telson around the joint between the peduncle and the fifth metasomal segment are situated proximally in the metasoma (Fig. 1).

Venoms are complex mixtures of different compounds including large proteins, peptides, small molecules and salts, injected into another organism. The high level of biological activity in venoms evolves in an arms-race of the source organism in defense against, or for incapacitation of, a specific class of target organisms (Barlow et al. 2009). Because scorpions rarely prey on vertebrates, compounds in scorpion venom that specifically bind to vertebrate targets (Pimenta et al. 2001; Bosmans et al. 2007) have presumably evolved for defensive purposes. Arthropod specific compounds (Arnon et al. 2005; Gurevitz et al. 2007) are likely targeted to prey species.

The stinging behavior in scorpions differs greatly between defensive and predatory strikes. For prey incapacitation, the stinger is only applied after the prey has been captured and is held securely with the chelae (Bub & Bowerman, 1979). The telson is then brought forward over the body by arching the metasoma as well as the mesosoma. Subsequently, the scorpion makes searching movements with its stinger, apparently probing for a soft spot to sting the prey. This probing may be guided by feedback from the several sensory organs on the cuticula (Foelix et al. 2014). This behavior is slow and highly controlled, and quite different from the rapid, quasi-ballistic projection of the stinger in defensive behavior, which takes only a fraction of a second. The vesicle of the telson may contact the attacker first, after which the aculeus is pushed forward by rotation of the telson (Zhao et al. 2016). The cuticle of arthropods is harder than the skin of most vertebrates. However, because scorpions search for the softer joints for stinging their

Correspondence
Arie van der Meijden, CIBIO Research Centre in Biodiversity and Genetic Resources, InBIO, Universidade do Porto, Campus Agrário de Vairão, Rua Padre Armando Quintas, N° 7, 4485-661 Vairão, Vila do Conde, Portugal. E: mail@arievandermeijden.nl

Accepted for publication *17 November 2016*
Article published online *28 December 2016*

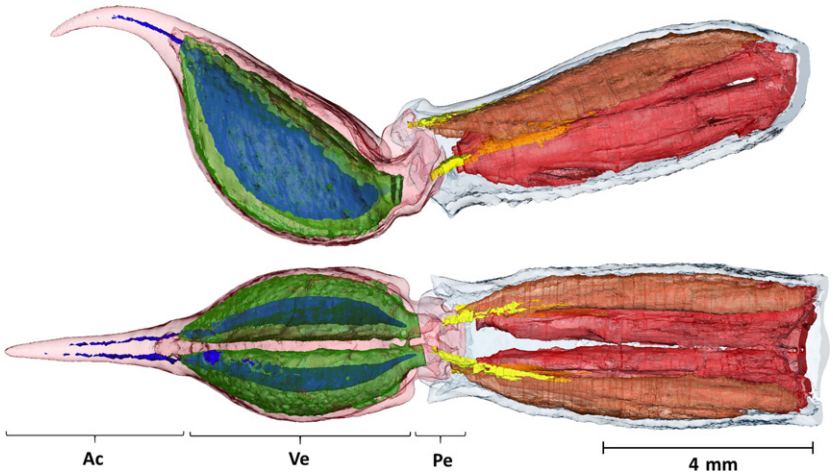

Fig. 1 Internal anatomy of the telson and the fifth metasomal segment (*Neochactas delicatus*). Top: lateral view; bottom: dorsal view. Cuticula of the fifth metasomal segment rendered in transparent blue, cuticula of the telson rendered in transparent pink. The telson can be subdivided into the aculeus (Ac), vesicle (Ve) and peduncle (Pe). Telson shows the venom gland (transparent green) and venom canal lumen (blue) inside the vesicle. The discontinuous lumen of the venom ducts may be due to coagulated venom existing inside the ducts. The thin layer of musculature around the venom glands is not shown. The apodemes are in yellow, and can be seen continuing inside the flexor (transparent brown) and extensor (transparent red) muscles. Note the larger volume of the extensor muscles, which allow a forceful extension of the telson in the direction of the aculeus tip. Scale bar: 4 mm.

arthropod prey, and vertebrate skin is very tough, defensive encounters in which both the scorpion and the predator struggle likely result in larger forces on the aculeus, and potentially at unexpected angles. The controlled stinging of prey is much less energetic and more predictable. We therefore expect that defensive encounters place the highest structural demands on telson. The stinging behavior in mating, in which the male stings the female during courtship, is also relatively slow and deliberate (Tallarovic et al. 2000), and more similar to the stinging behavior for prey incapacitation than to defensive stinging.

Further, we previously found large differences in the defensive use of the stinger between scorpion species (Van der Meijden et al. 2013). In defensive situations, some species depend more on the chelae, or are otherwise disinclined to sting. Defensive stinging behavior within a single species seems to also be dependent on body mass (Carlson et al. 2014) and temperature (Carlson & Rowe, 2009). Scorpions are thought to control the amount of venom they expel in encounters with predators (Nisani & Hayes, 2011), as venom regeneration may be costly (Nisani et al. 2007). The amount of venom injected during defensive behavior can be controlled by variation in flow rate and/or duration (van der Meijden et al. 2015). For stinger use during prey immobilization, an ontogenetic shift was found in two species of scorpions, *Pandinus imperator* and *Paruroctonus boreus* (Cushing & Matherne, 1980; Casper, 1985), with older specimens using the stinger less.

The diversity in telson use among different scorpion species and developmental stages is likely to be reflected in the shapes of the telsons as these differences in telson use are likely to change the mechanical demands on the venom delivery system. Analytical models by Zhao et al. (2016), similar to the findings of Bar-On et al. (2014), suggest that the optimal penetration angle of curved structures like scorpion aculei and spider chelicerae should minimize the normal stress, and maximize the structural stiffness in the telson cuticula. They found that this optimal angle shifts with the magnitude of the applied force, and is not parallel to the tip angle. Here we use 3D imaging and finite element analysis (FEA) to estimate the optimal load angles across a wide range of telson shapes from different scorpion taxa. By comparing the total strain energies under optimal static loading of the stinger, we test for performance differences across the diversity of telson shapes found in scorpions. This approach assumes the strain energy, and thereby the compliance of the structure, to be minimized in more mechanically resistant telson shapes. The relatively slow venom delivery in prey incapacitation seems less demanding on the structural robustness of the telson than the rapid defensive strike. Because scorpions that use their venom more in defensive behavior will likely have evolved venom that has a stronger effect on vertebrates, we expect telson morphology and FEA shape performance to correlate with venom effects on vertebrates.

Materials and methods

μCT scanning and segmentation

The telsons of ethanol-preserved scorpions of 33 species representing nine families were scanned with a Skyscan 1172 (Bruker MicroCT, Kontich, Belgium) desktop μCT scanner, and volumetric slices were reconstructed with NRecon 1.5, which is part of the

Skyscan software suite. One individual was scanned per species. Because of interspecific size differences, we adjusted the field of view of the μCT scanner for each specimen, which resulted in different resolutions for each scan (Table 1). Segmentation of the telson cuticula was performed in AMIRA 5.3.3 (FEI software). Polygonal surfaces were calculated in AMIRA from the segmented data and optimized as described in van der Meijden et al. (2012). We reduced the number of polygons until we could visually detect a decrease in the detail of the surface topography, remeshed the surface to increase the regularity of the polygon mesh, and used the AMIRA surface editing tools to deal with intersecting elements prior to the generation of a solid mesh that consisted of tetrahedral elements. Because the different species showed notable differences in their telson morphology, the resulting solid mesh models slightly differed in the number of tetrahedral elements (Table 1). To estimate the effect of differences in the total element count, we have randomly chosen two species from our dataset (Sc156 and Sc1630) and repeated all the analyses for models that were based on surfaces with 80%, 60%, 40% and 20% of the polygons compared with the original. We did not find any significant influence of mesh sizes on our results (Table S3).

FEA modeling and analysis

Solid mesh models were imported into PREVIEW 2.3, which is part of the open source FEA package FEBio (Maas et al. 2012). Each model was oriented by placing the axis of the joint around which the telson rotates on the *z*-axis, and the tip of the aculeus on the *x*-axis. The line between the tip of the aculeus and the center of the joint is hereafter referred to as the axis of the telson. The nodes at the base of the telson peduncle, including the attachment points of all apodemes and the joint, were constrained in rotation and translation in all degrees of freedom. The material was modeled as an isotropic elastic material, with a Young's modulus of 7e+009 and a Poisson's ratio of 0.33 (van der Meijden et al. 2012). A point load was applied to a single node at the tip of the aculeus, parallel to the *y*-axis. To make the results of the FEA directly comparable, despite size differences of the telsons in different species, we kept the ratio of point loads over the surface area of the solid meshes constant, scaling all point loads according to a force of 0.1 N relative to specimen 593. For constant force to surface area ratios, differences in the calculated stresses and strains among species directly reflect shape differences (Dumont et al. 2009). In order to test whether the direction of the load on the tip of the aculeus influenced the total stress in the telson cuticula, the angle of the telson axis was rotated around the axis of the joint in 10 ° increments over at least 120 °, and a FEA was performed with the non-linear solver of FEBio for each rotational step. From the FEBio output, we exported the values for effective stress σ, effective strain ε and volume V for each element. For an elastic material, the area under the stress–strain curve is a measure for the strain energy density u and can be calculated as:

$$u = \frac{1}{2}\sigma * \varepsilon. \quad (1)$$

Total strain energy describes the work of elastic deformation over all elements of the finite element models analyzed, and can be calculated by integrating strain energy density over the whole volume (Kelly, 2015). Based on this, we estimated the total strain energy U as in Eq. 2, with i as the number of each individual element and N as the total element count.

$$U = \sum_{i=1}^{N} V_i \times u_i. \quad (2)$$

Calculations were performed with the R statistics package version 3.1.3 (R Development Core Team, 2016). To directly compare total strain energies among species, we calculated a scaling factor that considers a constant ratio of the point load force over the sixth root of the model volume, in which case differences in the total strain energy are size independent (Dumont et al. 2009). This scaled total strain energy was calculated for each angle. Because energy that is stored in elastic deformation of the stinger is not available to

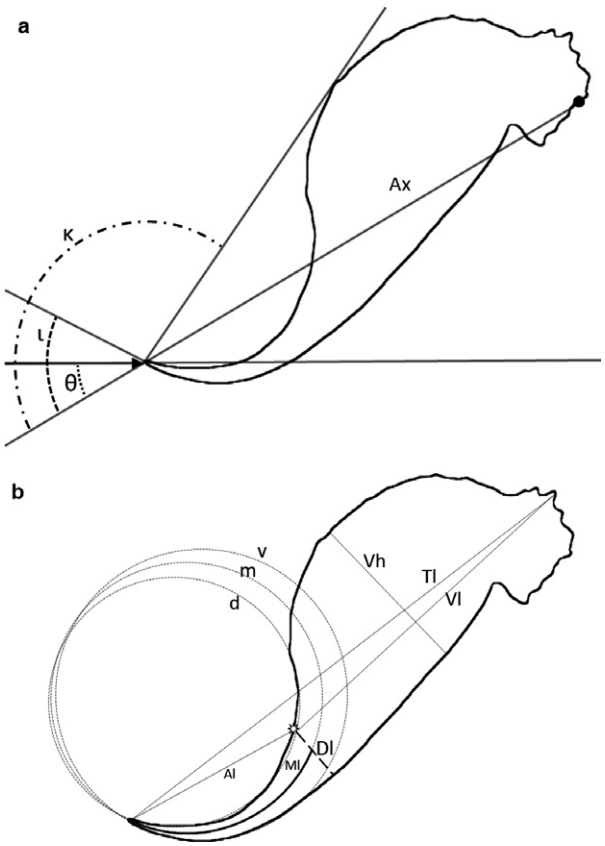

Fig. 2 Schematic of morphological measurements. (a) The horizontal arrow indicates the point load applied to the tip of the telson model. The optimal angle (θ) is the angle between the applied force where the FEA model shows the lowest strain energy and the line from the joint to the tip (telson axis). The tip angle (ι) was calculated using a polynomial fit to the midline of the aculeus at the tip (see text). The angle between the telson axis and the line from the tip to the highest point of the vesicle (κ). Ax indicates the telson axis, here defined as the line between the tip of the aculeus, and the center of the joint axis. The latter here is indicated with a black dot. (b) Total length (Tl), vesicle height (Vh) length (Vl) and circles fit to the ventral (v) and dorsal (d) outline of the aculeus, as well as to the midline (m). Star shows the point on the ventral outline where the aculeus starts, as based on the sharpest increase in height. Dl is the demarcation line between aculeus and vesicle (see text). Ml indicates the midline of the aculeus, the length of which was recorded as the arc length of the aculeus. Al is the linear length of the aculeus. Note that the stinger is shown here in the orientation in which it is used, with the ventral side up.

actually pierce the target, it seems reasonable to assume that total strain energy should be minimized during a stinger attack. A fifth order polynomial function was fit to the relationship between angle and scaled total strain energy, with an $R^2 > 0.9999$. The angle at which the minimal strain energy occurs (optimal angle, θ; Fig. 2), as well as the corresponding minimal strain energy, were estimated using this polynomial function. To visualize stress differences at the optimal angle, we then performed another FEA for each species with the telson oriented at its calculated optimal angle.

Morphology

In taxonomic studies, the aculeus is defined to start caudal from the pair of large setae on the ventral surface of the telson (Vachon, 1952), or the subaculear tubercle if present (Stahnke, 1970). However, these are often placed more on the bulbous part of the telson, and this definition of the starting point of the aculeus is decoupled from a functional distinction between the slender aculeus and swollen vesicle. We therefore defined the aculeus here to end at the point on the ventral surface where the dorsoventral height of the telson increases most rapidly, going from the tip of the aculeus to the base of the telson. In order to calculate the transition point between the aculeus and the vesicle, as well as several other morphological variables, the lateral view of the telson model was exported as an image. This image was then analyzed in Matlab 2015b (The Mathworks, Natick, MA, USA) using a custom script. First, the dorsal and ventral outlines of the stinger were traced. A polynomial function was then fit to the outlines, and increased in degree until the value of R^2 exceeded 0.999. Then 1000 equidistant points were calculated from the polynomials of the ventral and the dorsal outline. Pairwise distances between the points on the dorsal and ventral outlines were calculated, resulting in a 1000×1000 matrix. For each point on the ventral outline, the distance between that point and the closest point on the dorsal outline was taken as the local height of the telson. The largest of the local heights was recorded as the height of the vesicle for the specimens without a subaculear tubercle. The local height measurements were then used to define the point where the vesicle transitions into the aculeus by

Table 1 Used material and model variables.

	Family	Specimen number	Sex	Voxel size	# Elements	Mean edge length (μm)
Bothriurus coriaceus	Bothriuridae	1874	m	21.08	17 9761	35.8
Brachistosternus negrei	Bothriuridae	1090	m	13.86	18 4968	36.9
Androctonus australis	Buthidae	707	m	26.68	18 6496	60.6
Androctonus gonneti	Buthidae	1453	f	21.34	20 2964	60.5
Androctonus liouvillei	Buthidae	1055	f	26.68	19 9740	52.9
Babycurus jacksoni	Buthidae	1147	f	21.60	18 9784	59.2
Buthacus sp.	Buthidae	593	m	12.80	19 4999	30.4
Compsobuthus werneri	Buthidae	674	m	11.74	17 5973	29.4
Grosphus flavopiceus	Buthidae	881	m	26.68	20 2926	77.0
Isometrus petrzelkai	Buthidae	1632	f	11.74	18 0150	19.1
Leiurus quinquestriatus	Buthidae	1062	n.a.	21.60	18 5085	49.7
Mesobuthus martensi	Buthidae	678	m	16.27	19 0907	36.4
Microbuthus fagei	Buthidae	1578	f	12.80	18 9948	15.5
Orthochirus cf. *innesi*	Buthidae	156	n.a.	9.87	21 6337	23.5
Rhopalurus crassicauda	Buthidae	677	Subadult	9.87	20 1268	28.4
Tityus bahiensis	Buthidae	662	f	13.86	20 0823	33.3
Caraboctonus keyserlingi	Caraboctonidae	701	f	18.14	18 8040	52.6
Chactas sp.	Chactidae	999	f	20.00	18 6762	43.8
Neochactas delicatus	Chactidae	1852	n.a.	17.87	20 1601	40.3
Chaerilus celebensis	Chaerilidae	779	f	9.60	17 4889	29.8
Euscorpius flavicaudis	Euscorpiidae	879	f	8.80	17 2885	20.2
Iomachus politus	Hormuridae	1268	m	15.74	17 3705	29.6
Opisthacanthus asper	Hormuridae	1258	f	26.68	17 9756	48.8
Opisthacanthus maculatus	Hormuridae	877	f	17.60	17 3257	31.6
Paleocheloctonus pauliani	Hormuridae	2308	m	12.27	17 5582	27.1
Heterometrus petersii	Scorpionidae	1630	m	21.88	18 7659	76.3
Opistophthalmus boehmi	Scorpionidae	696	f	13.07	17 7981	32.3
Pandinus cavimanus	Scorpionidae	623	m	24.01	18 9196	68.5
Scorpio fuliginosus	Scorpionidae	605	f	19.46	19 3500	52.8
Hoffmannius spinigerus	Vaejovidae	658	m	11.74	21 5058	39.0
Paravaejovis sp.	Vaejovidae	1873	m	11.74	18 1232	32.4
Paruroctonus sp.	Vaejovidae	2152	m	18.94	26 7219	28.7
Smeringurus mesaensis	Vaejovidae	1863	m	14.93	18 9273	34.5

Specimen numbers refer to the accession number of the specimen in the specimen collection at the CIBIO institute, University of Porto.

identifying the point at which the dorsoventral height increases most rapidly (star in Fig. 2b). The line connecting this point, which lies on the ventral outline, and the closest point on the dorsal outline was considered the demarcation line between aculeus and vesicle. The distance from the middle of this demarcation line to the furthest point on the outline was recorded as the vesicle length. This demarcation line could not be defined for species with a subaculear tubercle, and for these four species no aculeus-related measurements were taken. Because several morphological measurements depend on the demarcation line between aculeus and vesicle, the species with a subaculear tubercle were not included in the statistical analyses.

After defining the border between the vesicle and the aculeus, several morphological measurements were made on the aculeus alone. First, to increase spatial resolution, 1000 points along the dorsal and ventral outlines were calculated from the polynomial for the aculeus only. The midline of the aculeus was defined to be half way between each point on the ventral outline, and the closest point on the dorsal outline. The length of the aculeus was measured as the linear distance from the tip to where the midline meets the demarcation line between aculeus and vesicle (linear aculeus length), and as the length of the arc described by the aculeus as measured along the midline (aculeus arc length). Because the arc of the aculeus can be approximated by a fraction of a circle, this was recorded as the arc angle of the aculeus. In order to calculate the radius of curvature of the aculeus, the instantaneous radius of curvature was calculated for each of 998 points along the ventral and dorsal outlines. The mean instantaneous radius of curvature was calculated using the trimmean function in Matlab. The mean instantaneous radius of curvature along the aculeus, as well as the standard deviations, is reported in Table S2. As a second estimate of the overall curvature of the aculeus, circles were fit to the ventral and dorsal outlines and the midline (Fig. 2b). As was done for the entire telson, the height of the aculeus was measured along its length. From this, the average dorsoventral height of the aculeus was calculated, as well as the height of the aculeus at its base.

Prior to further analysis, all morphological variables were corrected for telson size by dividing by telson length. Total length was

Surface area (m^2)	Volume (m^3)	Scaled forces (N)	Force per 6th root of volume	Total strain energy scaling factor	BB	vox
5.66E-05	3.36E-09	0.134	3.468	0.268	6977.09	332
6.25E-05	3.14E-09	0.148	3.874	0.240	6641.16	480
1.67E-04	1.79E-08	0.397	7.758	0.120	10 752.4	404
1.72E-04	1.35E-08	0.408	8.366	0.111	11 846.3	556
1.26E-04	1.37E-08	0.299	6.115	0.152	9258.27	348
1.59E-04	1.89E-08	0.377	7.304	0.127	8358.71	388
4.22E-05	1.82E-09	0.100	2.862	0.324	4288.82	336
3.99E-05	1.09E-09	0.0947	2.953	0.314	4683.26	400
2.89E-04	3.87E-08	0.686	11.796	0.0787	13 100.3	492
1.65E-05	3.82E-10	0.0391	1.452	0.639	5293.61	452
1.12E-04	6.87E-09	0.265	6.083	0.153	11 641.7	540
9.16E-05	1.31E-08	0.217	4.477	0.207	7859.15	484
1.05E-05	3.80E-10	0.0250	0.928	1.000	10 280.4	804
2.48E-05	1.20E-09	0.0589	1.808	0.513	5279.31	536
3.83E-05	1.43E-09	0.0909	2.708	0.343	4647.77	472
5.26E-05	3.05E-09	0.125	3.279	0.283	4811.03	348
1.32E-04	8.72E-09	0.313	6.900	0.134	9053.3	500
8.68E-05	6.24E-09	0.206	4.799	0.193	9740	488
7.40E-05	4.15E-09	0.175	4.378	0.212	5416.03	304
4.26E-05	1.36E-09	0.101	3.036	0.306	5711.65	596
1.89E-05	3.68E-10	0.0447	1.671	0.555	2490.71	284
3.93E-05	1.48E-09	0.0932	2.759	0.336	3320.59	212
1.07E-04	7.43E-09	0.253	5.733	0.162	5202.78	196
4.44E-05	1.71E-09	0.105	3.044	0.305	17 584.6	1000
3.34E-05	1.08E-09	0.0793	2.474	0.375	6368.41	520
2.73E-04	2.73E-08	0.649	11.823	0.0785	16 692.6	764
4.67E-05	1.82E-09	0.111	3.171	0.293	6049.52	464
2.22E-04	2.07E-08	0.527	10.057	0.0923	7754.36	324
1.31E-04	1.32E-08	0.312	6.417	0.145	13 215.8	680
7.36E-05	4.11E-09	0.175	4.362	0.213	9143.51	780
4.83E-05	1.86E-09	0.115	3.267	0.284	9894.71	844
3.66E-05	1.39E-09	0.0869	2.601	0.357	4148.12	220
5.51E-05	2.15E-09	0.131	3.638	0.255	5300.96	356

different from the measure usually used in taxonomy, as the μCT scans allowed us to measure the length from the tip to the furthest point on the telson, which may lie inside the body. The width of the vesicle was measured from the μCT scan data in Amira using the 3D measurement tool.

To quantify how strongly conical the aculei were, we defined the variable conicity as the ratio of the aculeus base height to the arc length. The variable tapering was defined as the mean height of the aculeus divided by half the height of the aculeus base. In a linearly tapering shape, this value would be 1. Higher values indicate that the most rapid tapering tends to be toward the end of the aculeus, whereas values lower than 1 indicate more tapering at the base. This assumes the aculeus does not increase in height from the base to the tip.

The axis of the telson is here defined as the line between the tip of the aculeus and the center of the rotation axis of the joint at the telson peduncle. The rotation axis passes through the two joints at either side of the peduncle. Three angles were quantified, all relative to the axis of the telson (Fig. 2a). The angle at the tip of the aculeus (ι) was calculated from the tangent line of the polynomial function fit to the midline of the aculeus. Zhao et al. (2016) observed the vesicle first contacting the target, after which the telson was rotated so the tip started to penetrate the target. In this situation, the penetration angle would be the angle between the telson axis and a line from the tip of the telson to the outline of the vesicle. A line was drawn from the tip of the aculeus, and rotated toward the vesicle until it contacted the outline of the vesicle (angle κ), which is perpendicular to the penetration angle of the tip in the situation described by Zhao et al. (2016). The angle θ is the optimal angle based on the FEA modeling, as described above.

For presentation, a hierarchical clustering was performed in R based on Euclidian distance. Distances were calculated based on morphological variables: telson height, width, vesicle length, aculeus length along the midline, and radius of the circle fit to the aculeus midline, all scaled by total telson length. In addition, the expectation maximization algorithm was used to detect the number of distinct clusters under the BIC criterion using the R package MCLUST. This resulted in 28 clusters. Because this large number of clusters would not be informative, the four highest order clusters were selected from the hierarchical clustering for presentation and referred to as clusters A–D (Fig. 3). Because these clusters were not supported by the expectation maximization algorithm, we did not use these clusters in the analysis. As it was not possible to define the point between the aculeus and the vesicle for the species that have a subaculear tubercle, these were not included in the clustering, and are shown separately in Fig. 3.

For lack of sufficient LD_{50} data in the literature for the species in this study, we used the four category system from Stockmann & Ythier (2010) to classify the potency of the venom for humans. Ythier and Stockmann classify scorpion species as 'low-toxicity', 'moderate toxicity', 'toxic' and 'very toxic, possibly lethal'. For species for which no classification was available, the classification of a closely related species in the same genus was selected. Although this classification is rather subjective and pertains only to the risk a species may cause in humans, no more quantitative data are available in the literature for all species in this study.

Statistical analysis

Statistical analyses were carried out in R (R Development Core Team, 2011) on the 29 species without a subaculear tubercle. A multiple regression was performed with optimal angle (θ) and minimal energy as dependent variables, and selected morphological variables as independent variables (Table 2). Independent variables with a covariance with other independent variables greater than 0.8 were excluded from the multiple regressions to avoid multicollinearity (Table 2). In order to take the phylogenetic history into account, we used the phylogeny published by Sharma et al. (2015) for phylogenetically informed statistics. Because not all taxa we studied were included by Sharma et al. (2015), we added the missing taxa to that tree based on their relative taxonomic position. When placement was ambiguous, the grouping was presented as a polytomy. The resulting tree is shown in Fig. 4. Only the topology was used in further analysis. Polytomies were randomly broken up into several dichotomies with zero length branches (function Multi2di in R package Ape). All other branches were assigned a branch length of 1. Phylogenetic independent contrasts were calculated using the Pic function in the APE package (Paradis et al. 2004). To test if any of the functional or morphological characters differ significantly between venom potency groups, we performed phylogenetic ANOVAS using the Phy.anova function in the GEIGER package (Harmon et al. 2008) with 1000 simulations.

We calculated Pagel's λ as a measure for phylogenetic signal, as it is relatively robust to lack of branch lengths and presence of polytomies (Münkemüller et al. 2012). The Phylosig function in the Phytools R package (Revell, 2012) was used to calculate λ for all morphological variables as well as minimal strain energy and optimal angle (θ).

Results

FEA models

All 33 FEA models showed a concentration of stress at the tip of the aculeus (Fig. 3). A few species, such as the representatives of *Leiurus*, *Buthacus*, *Mesobuthus*, *Rhopalurus* and *Grosphus* also showed high stress at the base of the aculeus. These species have an aculeus that is not very conical. No such basal stress concentrations were seen in more conical shaped aculei, such as those of the species in group C. Stress was higher along the ventral and dorsal surfaces of the aculeus, as could be expected based on beam theory. Stress was also concentrated around the base of the vesicle near the peduncle in most species, but this may be an artifact of the boundary conditions at the base of the telson. Optimal angles θ, i.e. orientations of the telsons in the FEA to minimize total strain energy, ranged from 11 ° to 56 ° (Table S2; see Table S1 for strain energies at other angles).

Morphology

We found considerable variation in telson morphology, as summarized in Table S2. We found that not all aculei are well described by a circle arc, but varied in their instantaneous curvature at different points along the aculeus. This is reflected in the standard deviation in the instantaneous radius of curvature. Most aculei did not describe a 90 ° arc, but varied between 44 ° (*Microbuthus*) and 116 °

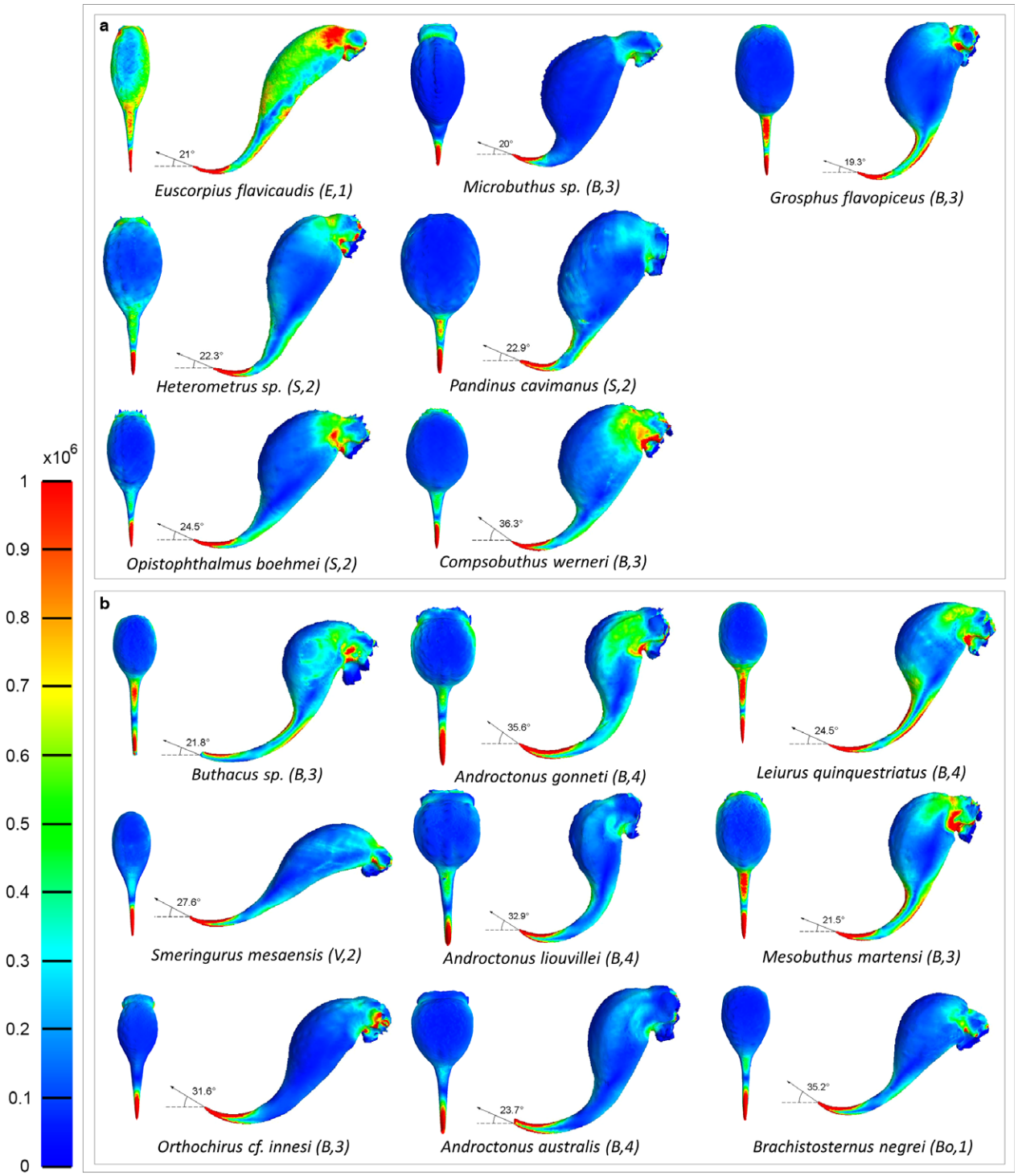

Fig. 3 (two panels) Telsons grouped by relative height, width, vesicle length, aculeus length and radius of curvature of the aculeus. Groupings are indicated by boxes [(a,b),(c,d)]. Telsons with a subaculear tubercle were not included in the clustering. The name is followed by a letter and a number in brackets, indicating family and venom group, respectively (1–4, low to high toxicity). (Bo) Bothriuridae, (B) Buthidae, (Ca) Caraboctonidae, (Ch) Chactidae, (C) Chaerilidae, (E) Euscorpiidae, (H) Hormuridae, (S) Scorpionidae, (V) Vaejovidae. All telsons are shown with optimal angle as a horizontal line, and tip angle as an arrow. Scale bar indicates effective stress (Pa). Sizes not to scale.

(*Heterometrus petersi*), with a mean of 75.5 °. Also, the angle of the tip (ι) did not make a 90 ° angle with the axis of the telson, as would be expected if the tip angle of attack lies on the tangent of the arc described by the telson around its joint. Rather, ι varied between 42 ° (*Smeringurus mesaensis*) and 84 ° (*Isometrus petrzelkai*), with a mean of 62 °.

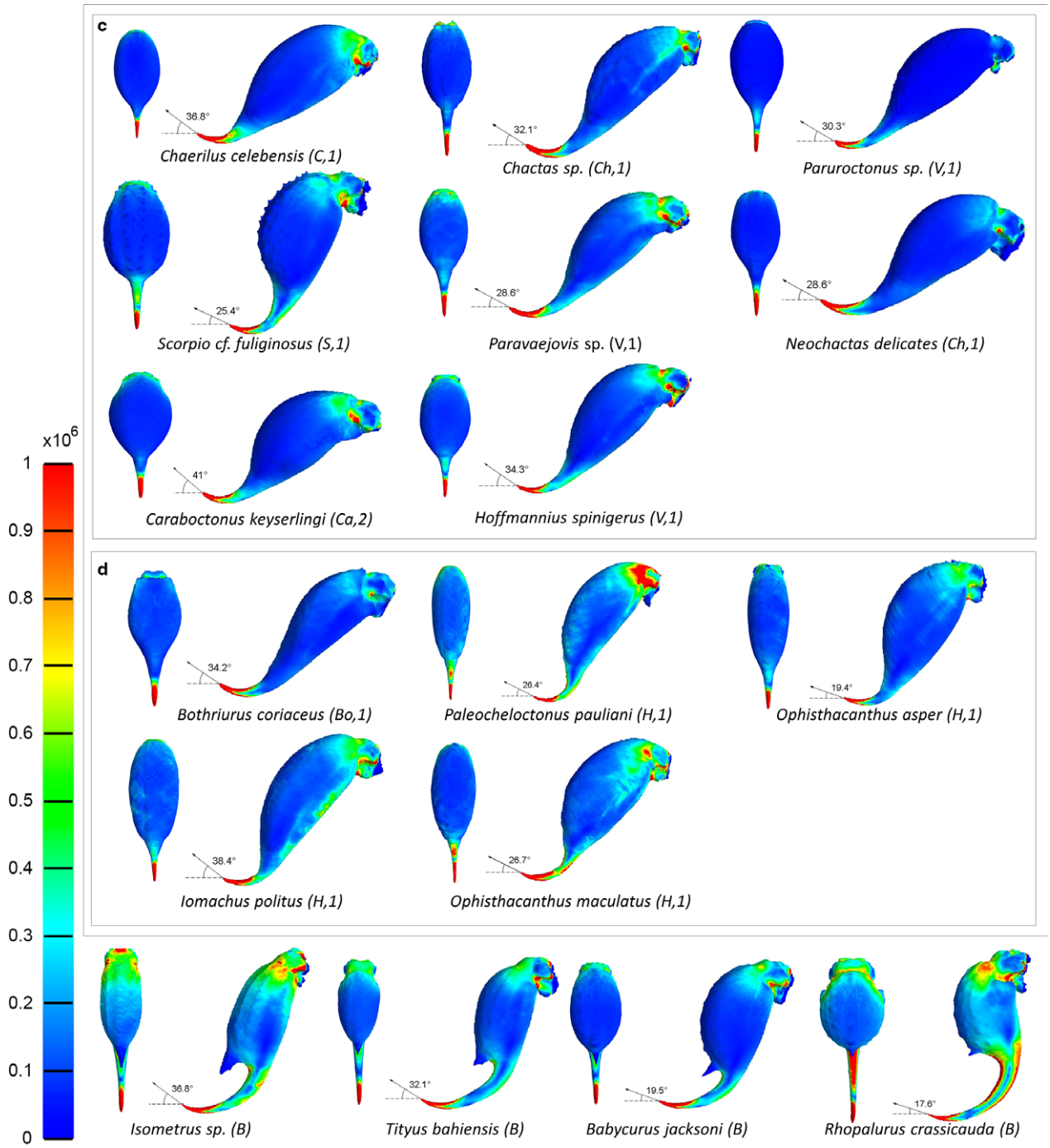

Fig. 3 Continued.

Statistical results

Multiple regression with optimal angle (θ) as the dependent variable and morphological variables scaled by telson length as independent variables showed, among others, a strong relationship between θ and the tip angle (ι) ($P < 0.001$; Table 2). The mean angle between them was 28.4 ± 6.22 °. Multiple regression of independent contrasts also recovered several significant relationships between optimal angle (θ) and several morphological variables, as did minimal strain energy (Table 2).

The mean height of the aculeus, the radius of the circle fit to the midline, as well as that of the dorsal outline of the aculeus, showed phylogenetic signal.

Phylogenetic ANOVAs found differences between the four venom potency groups. The morphological variables

Table 2 Results of statistical tests.

					Multiple regressions				Independent contrasts			
	Phylogenetic signal		Phylogenetic ANOVAS		Optimal angle θ		Min energy		Optimal angle θ		Min energy	
Variable	λ	p	f	p	Coeff	p	Coeff	p	Coeff	p	Coeff	p
Minimal strain energy	6.61E-05	1.00E+00	1.90E+00	2.04E-01	−0.05	4.5E-01			−0.13	2.4E-02		
Optimal angle θ	6.44E-01	9.91E-02	9.07E-01	5.16E-01			−0.87	4.5E-01			−2.39	2.4E-02
Tip angle ι	7.52E-01	1.45E-01	6.77E-01	6.50E-01	−0.84	2.3E-09	−1.07	2.7E-01	−0.89	4.0E-10	−2.58	5.5E-03
Tip-vesicle angle κ	5.58E-05	1.00E+00	3.13E-01	8.76E-01	−0.50	6.4E-07	−0.76	2.1E-01	−0.59	8.3E-09	−1.56	1.5E-02
Linear length aculeus	1.00E+00	4.12E-03	1.28E+01	9.99E-04	0.55	2.8E-01	4.03	4.9E-02	0.23	4.5E-01	1.68	1.9E-01
Aculeus arc length	1.00E+00	6.32E-03	1.19E+01	9.99E-04								
ArcAngle	1.85E-02	9.19E-01	1.65E+00	2.70E-01	−0.36	7.9E-02	−0.84	3.5E-01	−0.32	1.5E-01	−1.98	3.0E-02
Aculeus base height	7.00E-01	1.10E-01	7.43E+00	4.00E-03	0.27	3.8E-01	1.75	1.7E-01	0.35	6.8E-02	1.91	1.5E-02
Aculeus conicity	7.47E-01	1.40E-01	1.35E+00	3.25E-01	0.03	9.4E-01	−1.74	2.8E-01	−0.66	4.8E-02	−3.47	1.2E-02
Aculeu tapering	6.61E-05	1.00E+00	2.72E+00	7.99E-02	0.10	6.3E-01	−0.42	6.5E-01	−0.42	3.3E-02	−2.12	9.3E-03
Mean aculeus height	1.00E+00	4.03E-04	9.28E+00	2.00E-03	−0.03	9.2E-01	−2.29	4.9E-02	−0.06	4.1E-01	−0.64	2.7E-02
Mean radius of curvature	3.49E-01	9.69E-02	7.10E+00	9.99E-04								
Radius circle dorsal	1.00E+00	3.03E-05	1.84E+01	9.99E-04								
Radius circle midline	1.00E+00	3.85E-05	1.78E+01	9.99E-04	−0.61	1.2E-01	−1.55	3.7E-01	−0.27	2.7E-01	−1.40	1.7E-01
Radius circle ventral	1.00E+00	5.45E-03	8.98E+00	9.99E-04								
Vesicle height	1.40E-01	7.43E-01	5.84E-01	7.05E-01	−0.17	2.0E-02	−0.06	8.7E-01	−0.21	2.2E-03	−0.34	3.1E-01
Vesicle length	9.99E-01	1.16E-02	9.80E+00	9.99E-04								
Vesicle width	6.61E-05	1.00E+00	9.66E-01	4.91E-01	0.00	9.7E-01	0.07	8.1E-01	0.03	6.6E-01	0.18	4.9E-01
Venom group	6.04E-01	3.21E-02										
Multiple R^2						0.98		0.70		0.99		0.80
P						5.6E-10		6.2E-02		3.7E-11		7.9E-03

Regressions of variables and contrasts are shown with standardized coefficients. *P*-values in bold are significant at a value of alpha of 0.05, after Bonferroni correction.

pertinent to the relative length of the aculeus were found to differ significantly between venom potency groups after Bonferroni correction (Fig. 5; Table 3). All variables relating to the radius of curvature of the aculeus varied with venom potency group. Aculeus base height also differed between venom groups, but this was not significant at a value of alpha of 0.05 after Bonferroni correction. Scaled minimal strain energy and optimal angle did not differ significantly between venom groups.

Discussion

No relationship between minimal strain energy and venom group

We expected species in the highest venom potency groups to exhibit a telson shape better able to withstand the impact of the fast defensive strikes. We expected this to be evident by the telsons in these groups exhibiting a lower scaled minimal strain energy. However, no such relationship was found in the phylogenetic ANOVAS. This could be due to the assumption of a larger impact force, due to the higher velocity in defensive strikes, being false. Force measurements could test this assumption, and shed light on the ecological functions affecting telson shape. The assumption that minimal strain energy is optimized under conditions of high loading force may also be false.

Risk of breakage

The minimal strain energy, the strain energy in the telson cuticula when loaded at the optimal angle, showed a positive relationship with aculeus length and a negative one to aculeus height. This seems to indicate that short thick aculei incur less strain. This relationship did not become apparent with the related aculeus conicity or tapering variables.

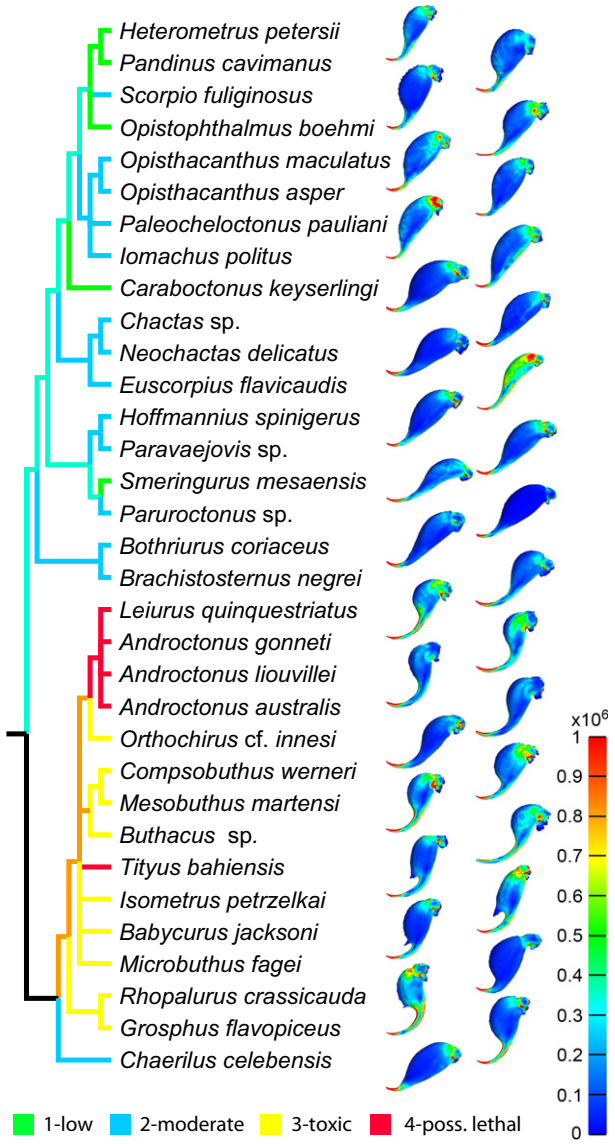

Fig. 4 Cladogram used for phylogenetically informed statistics based on Sharma et al. (2015). See 'Statistical analysis' for details. Taxa for which placement was ambiguous were left as polytomies. The color of branches indicates venom group. Intermediate colors indicate branches of which the terminal taxa belong to more than one venom group. Telson colors indicate effective stress (scale bar, Pa). Sizes not to scale.

However, because strain energy was calculated for the entire telson, other factors could cause this relationship.

Species with a stress concentration at the base of the aculeus in the FEA models are among the species in the highest venom potency classes, and some of these are known to have a high defensive use of the stinger (van der Meijden et al. 2013). Species such as those of the genus *Androctonus*, have extremely muscular metasomas, capable of delivering the telson with significant force. These scorpions can sometimes launch themselves backward when hitting a large object with the aculeus, accelerating their entire body (personal observation AvdM). It is therefore remarkable that the telson of these species has an aculeus that is not very conical (*Androctonus* aculeus conicity of 0.19–0.23). Having a more conical shape would reduce the stress concentrations at the base of the aculeus, and have a smaller chance of breakage (Bar-On et al. 2014). Breakage of the tip is preferable, as the aculeus is still usable with a slightly truncated tip. We have encountered scorpions in the field with broken aculei, ranging from a truncated tip to a missing aculeus. The mean aculeus height, a measure of the thickness of the aculeus along its length, is higher in the more venomous species. This design does not negate the potential of breakage of the aculeus at the base, but reduces the chance of breakage altogether. It is unclear why the more venomous species would have an aculeus shape that has less chance of breakage, but in which any breakage could occur catastrophically at the base of the aculeus. It is possible that the risk of breakage at the base is compensated with superior material properties in these species. This would not be evident using the approach employed here, as we designed our study to isolate the effects of differences in shape alone, irrespective of variability in material properties. However, it remains unclear what benefit these longer aculei have in delivering venom over the more conical shape of less venomous species. One possibility is the increased penetration depth offered at reduced resistance. We have hitherto not observed these species injecting their prey more deeply than species with more conical aculeus designs. Typically, only a small fraction of the aculeus length is inserted into the prey for prey incapacitation. It is conceivable that long aculei allow easier penetration of dense fur coats or feathers in defensive use. Because the species having such long aculei also carry venom effective in vertebrates, as evident from the high correlation of telson length to venom potency, these long aculei may be adaptive for deterrence of vertebrate predators. Behavioral observations of encounters with predators therefore will be necessary to substantiate the conjecture that longer aculei facilitate defensive use of the telson. Also, the assumption here, and often implicit in studies of venom efficacy, is that a strong effect on humans signals a strong effect on vertebrates, or even all animals generally. Whether effects in humans are a reliable indicator for the ecologically relevant defensive potential of the venom of a particular species of scorpion remains to be tested. Known development of insensitivity to venom by predators (Holderied et al. 2011; Rowe et al. 2013) makes this assumption unlikely to hold in all cases.

Strain energy and κ

Zhao et al. (2016) described a single defensive strike with the vesicle first contacting the surface of the simulated predator, followed by insertion of the aculeus by a rotation of the telson. If this mode of defensive stinging was the norm for defensive stings, and telson morphology is

adapted to minimize strain energy, then we would expect an association of κ with optimal angle. A relationship of optimal angle to κ was recovered. Because not all species in this study are equally likely to use the stinger in defensive situations, the association of κ to optimal angle may be strongest in species that use their venom more defensively. However, no significant difference in κ was found between venom groups.

Function of the subaculear tubercle

Interestingly, of the four species with a subaculear tubercle, this subaculear tubercle did not cross the line from the tip of the aculeus to the top of the vesicle (Fig. 2a). If the telson would be applied to a surface as described above, the subaculear tubercle would not touch the surface. It therefore cannot function as an alternative pivot point to guide the initial penetration of the aculeus. However, very pronounced subaculear tubercles may contact the surface after the tip has been sunk into the surface. For this scenario the aculeus would have to be sunk into the surface of a predator very deeply, which is unlikely to occur in our experience. The function of the subaculear tubercle remains unclear, and may lie in the other ecological functions of the telson, such as intraspecific antagonism, mating or even locomotion.

Tip angle and optimal angle

The association between tip angle and optimal angle was significant, also using independent contrasts. This suggests a functional relationship. The angle between the optimal angle from the FEA models and the tip angle (28.4 ± 6.22 °) suggests that the aculeus is not applied parallel to the tip angle, but at an angle. Such an angle may optimize the stiffness of the structure (Bar-On et al. 2014; Zhao et al. 2016), and is dependent on stinger shape and might also depend on the applied force (which was not tested herein). However, whether scorpions actually prefer to apply their stinger at the optimal angle will need to be verified with comparative behavioral studies.

Limitations and considerations

Zhao et al. (2016) modeled the stinger as describing a quarter circle. Our data show that future models may need to

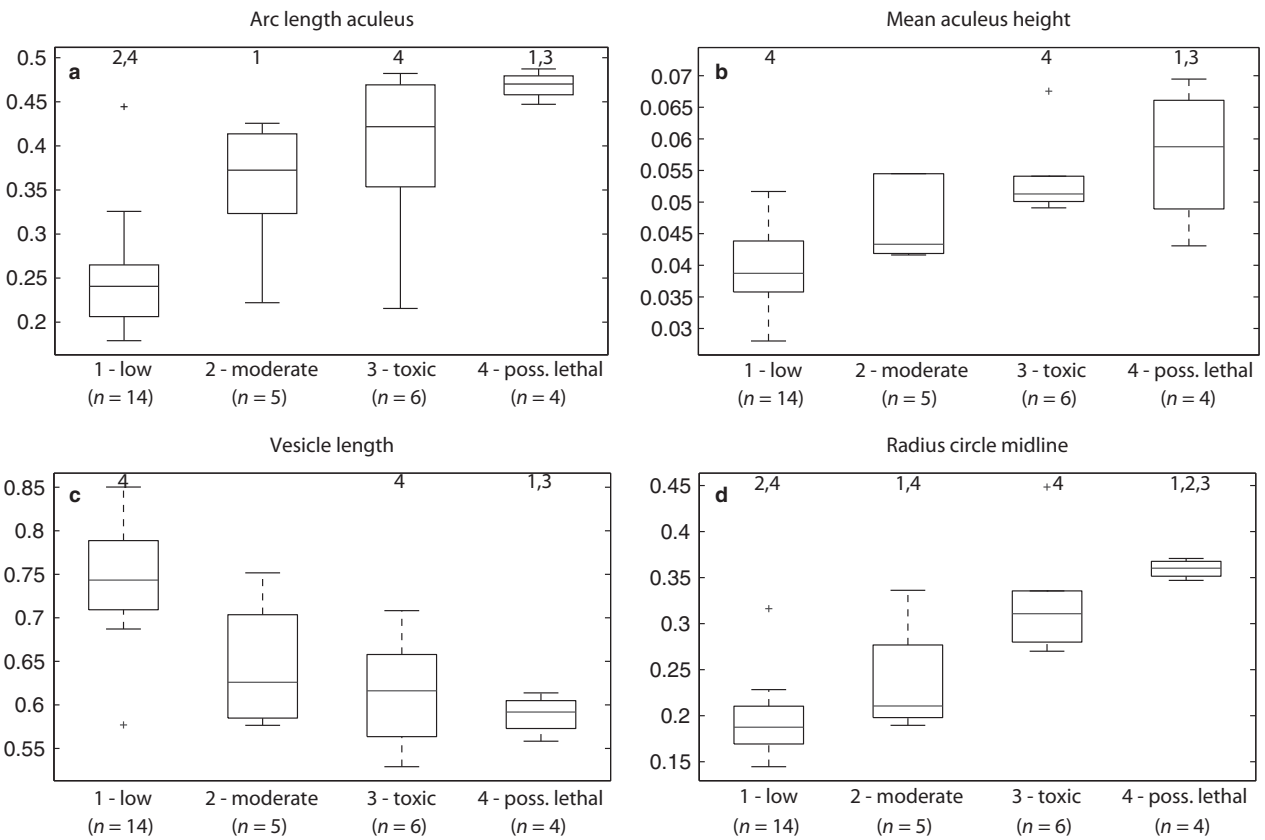

Fig. 5 Scaled morphological characters grouped by venom group (horizontal axes). These and other morphological variables showed a significant difference between venom groups. Numbers above boxes indicate groups with which there is a pairwise significant difference (*t*-test, $\alpha < 0.05$). (a) Arc length of the aculeus, (b) mean aculeus height, (c) vesicle length, (d) radius of the circle fit to the midline of the aculeus.

describe larger and smaller arcs to describe more accurately the variability in this parameter. Also modeling the curvature of the aculeus as a section of a circle may be an oversimplification. Some species diverged to a fair degree from a circular arc, as can be seen from the low value of R^2 of the circle fit (Table S2), as well as the relatively high standard deviation of the radius of curvature along the aculeus.

The chosen boundary conditions, immobilizing the proximal part of the peduncle in all six degrees of freedom, probably do not reflect the constraints on the telson during a stinging event. Under natural circumstances the loading of the telson may be reduced due to some amount of flexibility in the hinge, as well as the metasoma. Although the intraspecific variability is probably much lower than the differences between the species selected in this study, the use of a single specimen to estimate the properties of a species may not be representative, particularly in species that exhibit sexual dimorphism. For instance, the telson of *Euscorpius flavicaudis* used in this study belongs to a female specimen. The males of this species have a very differently shaped telson, which is used in courtship. As in this case the male telson is clearly the product of sexual selection, we chose the female to represent this species. In the other studied species, telson shape varies little between the sexes.

Isolating shape

It is important to note that our study does not take the potential anisotropy of material properties into account. Also, our value of Poisson's ratio and Young's modulus may not realistically describe the mechanical properties for each telson or its parts. Hardness is known to vary along the telson due to the inclusion of metalloproteins (Schofield, 2001) and, as hardness changes, so might Young's modulus. Rather, our study aims to highlight the differences in performance due to shape alone. The absolute values of stresses are therefore not relevant to biological telsons. By comparing shape alone, in isolation of material properties, realistic loading conditions or size, we can understand the relative importance of this aspect of the function of the telson. By isolating shape from material properties and size, we found significant patterns in telson shape evolution, and a potentially functional relationship between venom efficacy and telson shape. Whether more fragile shapes are compensated with superior material properties remains to be studied.

Acknowledgements

The authors thank Arendo Flipse and Bas van Ravenhorst for providing some of the scorpions used in this study. The authors are grateful to Pedro Sousa for identifying some of the specimens, and thank Pedro Coelho and Mykola Rasko for helpful suggestions. The authors are also grateful to Stanislav Gorb who provided access to the micro-CT scanner. AvdM is supported by a grant by Fundação para a Ciência e Tecnologia (FCT, Portugal) under the Programa Operacional Potencial Humano – Quadro de Referência Estratégico Nacional funds from the European Social Fund and Portuguese Ministério da Educação e Ciência (SFRH/BPD/101057/2014). This work is funded by FEDER funds through the Operational Program for Competitiveness Factors - COMPETE and by National Funds through FCT - Foundation for Science and Technology under the project FCT-PTDC/BIA-EVF/2687/2012 and FCOMP-01-0124-FEDER-028340.

Competing interests

No competing interests declared.

Author contributions

AvdM designed the study, carried out all morphological measurements, segmented the μCT data, performed statistical analysis and wrote parts of the manuscript. TK scanned the specimens, created solid mesh models, designed the FEA workflow, calculated all strain energies and wrote parts of the manuscript.

References

Arnon T, Potikha T, Sher D, et al. (2005) BjalphaIT: a novel scorpion alpha-toxin selective for insects – unique pharmacological tool. *Insect Biochem Mol Biol* **35**, 187–195.

Barlow A, Pook CE, Harrison RA, et al. (2009) Coevolution of diet and prey-specific venom activity supports the role of selection in snake venom evolution. *Proc Biol Sci R Soc* **276**, 2443–2449.

Bar-On B, Barth FG, Fratzl P, et al. (2014) Multiscale structural gradients enhance the biomechanical functionality of the spider fang. *Commun Nat*, **5**, 3894.

Bosmans F, Martin-Eauclaire M-F, Tytgat J (2007) Differential effects of five "classical" scorpion beta-toxins on rNav1.2a and DmNav1 provide clues on species-selectivity. *Toxicol Appl Pharmacol* **218**, 45–51.

Bub K, Bowerman RRF (1979) Prey capture by the scorpion *Hadrurus arizonensis* Ewing (Scorpiones: Vaejovidae). *J Arachnol* **7**, 243–253.

Carlson BE, Rowe MP (2009) Temperature and desiccation effects on the antipredator behavior of *Centruroides vittatus* (Scorpiones: Buthidae). *J Arachnol* **37**, 321–330.

Carlson BE, McGinley S, Rowe MP (2014) Meek males and fighting females: sexually-dimorphic antipredator behavior and locomotor performance is explained by morphology in bark scorpions (*Centruroides vittatus*). *PLoS One* **9**, e97648.

Casper GS (1985) Prey capture and stinging behavior in the emperor scorpion, *Pandinus imperator* (Koch) (Scorpiones, Scorpionidae). *J Arachnol* **13**, 277–283.

Cushing BS, Matherne A (1980) Stinger utilization and predation in the scorpion *Paruroctonus boreus*. *Great Basin Nat* **40**, 193–195.

Dumont ER, Grosse IR, Slater GJ (2009) Requirements for comparing the performance of finite element models of biological structures. *J Theor Biol* **256**, 96–103.

Foelix R, Erb B, Braunwalder M (2014) Fine structure of the stinger (aculeus) in *Euscorpius*. *J Arachnol* **42**, 119–122.

Gurevitz M, Karbat I, Cohen L, et al. (2007) The insecticidal potential of scorpion beta-toxins. *Toxicon* **49**, 473–489.

Harmon LJ, Weir JT, Brock CD, et al. (2008) GEIGER: investigating evolutionary radiations. *Bioinformatics* **24**, 129–131.

Holderied M, Korine C, Moritz T (2011) Hemprich's long-eared bat (*Otonycteris hemprichii*) as a predator of scorpions: whispering echolocation, passive gleaning and prey selection. *J Comp Physiol A* **197**, 425–433.

Kelly P (2015) Solid mechanics part I: an introduction to solid mechanics. URL http://homepages.engineering.auckland.ac.nz/~pkel015/SolidMechanicsBooks/Part_I/index.html

Maas SA, Ellis BJ, Ateshian GA, et al. (2012) FEBio: finite elements for biomechanics. *J Biomech Eng* **134**, 11 005.

van der Meijden A, Coelho P, Rasko M (2015) Variability in venom volume, flow rate and duration in defensive stings of five scorpion species. *Toxicon* **100**, 60–66.

Van der Meijden A, Lobo Coelho P, Sousa P, et al. (2013) Choose your weapon: defensive behavior is associated with morphology and performance in scorpions. *PLoS One* **8**, e78955.

van der Meijden A, Kleinteich T, Coelho P (2012) Packing a pinch: functional implications of chela shapes in scorpions using finite element analysis. *J Anat* **220**, 423–434.

Münkemüller T, Lavergne S, Bzeznik B, et al. (2012) How to measure and test phylogenetic signal. *Methods Ecol Evol* **3**, 743–756.

Nisani Z, Hayes WK (2011) Defensive stinging by *Parabuthus transvaalicus* scorpions: risk assessment and venom metering. *Anim Behav* **81**, 627–633.

Nisani Z, Dunbar SG, Hayes WK (2007) Cost of venom regeneration in *Parabuthus transvaalicus* (Arachnida: Buthidae). *Comp Biochem Physiol A Mol Integr Physiol* **147**, 509–513.

Paradis E, Claude J, Strimmer K (2004) APE: analyses of phylogenetics and evolution in R language. *Bioinformatics* **20**, 289–290.

Pimenta AMC, Martin-Eauclaire M-F, Rochat H, et al. (2001) Purification, amino-acid sequence and partial characterization of two toxins with anti-insect activity from the venom of the South American scorpion *Tityus bahiensis* (Buthidae). *Toxicon* **39**, 1009–1019.

R Development Core Team. (2016) *R: A Language and Environment for Statistical Computing*, R Foundation for Statistical Computing, Vienna, Austria. URL https://www.R-project.org/

Revell LJ (2012) phytools: an R package for phylogenetic comparative biology (and other things). *Methods Ecol Evol* **3**, 217–223.

Rowe AH, Xiao Y, Rowe MP, et al. (2013) Voltage-gated sodium channel in grasshopper mice defends against bark scorpion toxin. *Science* **342**, 441–446.

Schofield RMS (2001) Metals in cuticular structures. In: *Scorpion Biology and Research*. (eds Brownell PH, Polis GA), pp. 234–256. New York: Oxford University Press.

Sharma PP, Fernandez R, Esposito LA, et al. (2015) Phylogenomic resolution of scorpions reveals multilevel discordance with morphological phylogenetic signal. *Proc Roy Soc B Biol Sci* **282**, 20142953.

Stahnke HL (1970) Scorpion nomenclature and mensuration. *Entomol News* **81**, 297–316.

Stockmann R, Ythier E (2010) *Scorpions of the World*. NAP Editions. Verrieres-le-Buisson: France.

Tallarovic SK, Melville JM, Brownell PH (2000) Courtship and mating in the Giant Hairy Desert Scorpion, *Hadrurus arizonensis* (Scorpionida, Iuridae). *J Insect Behav* **13**, 827–838.

Vachon M (1952) *Etudes Sur Les Scorpions*. Algiers: Institut Pasteur d'Algérie.

Zhao Z-L, Shu T, Feng X-Q (2016) Study of biomechanical, anatomical, and physiological properties of scorpion stingers for developing biomimetic materials. *Mater Sci Eng C Mater Biol Appl* **58**, 1112–1121.

Supporting Information

Additional Supporting Information may be found in the online version of this article:

Table S1. Total strain energy scaled (Nm) for each angle of attack (°).

Table S2. Biomechanical and morphological variables. All size measurements are in mm. Venom group following the four class system of Stockmann & Ythier (2010) to classify the potency of the venom for humans: 1, 'low-toxicity'; 2, 'moderate toxicity'; 3, 'toxic'; and 4, 'very toxic, possibly lethal'. Asterisk indicates where a value of a closely related species was used. Some morphological variables could not be measured for species with a subaculear tubercle (see text).

Table S3. Mesh sensitivity analysis.